Applied Physics A (2024) 130:575
https://doi.org/10.1007/s00339-024-07721-2

Resistive switching behaviour in ZrO_2-CNT nanocomposite film

Aman Sharma[1] · **Mohd Faraz**[1,2] · **Neeraj Khare**[1]

Received: 7 December 2023 / Accepted: 8 July 2024 / Published online: 22 July 2024

Abstract
Resistive Random Access Memory (ReRAM) devices are being regarded as very promising choices for the future of non-volatile memory technology. The subject comprises crucial components like as material engineering, device architectural optimization, switching mechanisms, and improvements in reliability. This study examines the resistive switching capabilities of a device made from a ZrO_2-CNT nanocomposite. The device was constructed utilizing a trilayer structure consisting of FTO/ZrO_2-CNT/Ag, with the ZrO_2-CNT film being fabricated by the spray coating technique. Incorporating 1wt% CNT into the ZrO_2 matrix reduces the bias voltage needed for resistive switching and approximately doubles the resistance ratio between HRS and LRS. The use of higher weight percentages of carbon nanotubes (CNT) negatively impacts the switching properties. The temperature dependence of resistance of ZrO_2 and ZrO_2-1wt% CNT devices reveals that in ZrO_2, O_2 vacancies align to create conducting filaments. On the other hand, in the ZrO_2-CNT device, both vacancies of O_2 atoms and CNTs contribute to the production of conducting filaments. Inclusion of higher weight percentages of carbon nanotubes (CNT) leads to the formation of permanent conduction paths, which are electrical shorts and results in the loss of the switching capability.

Keywords ZrO_2 · High resistive state · Low resistive state · Resistance-temperature measurement · Resistive random access memory device

1 Introduction

The crucial significance of data storage devices is essential to the operation of computer systems. More precisely, the memory devices used in these systems require high density and fast access time [1–3]. Resistive switching devices have emerged as a transformative class of electronic components, offering a novel approach to non-volatile memory technology. As a result of the need for better nonvolatile memory solutions, researchers are now concentrating on resistive random access memory (ReRAM) devices [4]. These devices possess favorable characteristics, including a simple design, low power consumption, and high density, which make them viable contenders for the next generation of non-volatile memory technologies [5]. In a ReRAM device, when a suitable voltage is applied across the electrodes, the device switches reversibly between the high resistance state (HRS) and the low resistance state (LRS) [6–8]. ReRAM device consists of a trilayered Metal-insulator/Semiconductor-Metal (MIM) structure for the resistive switching phenomenon [9]. Resistive switching, an essential phenomenon for non-volatile memory applications, occurs in several materials such as oxide materials [10–12], organic polymer [13], and chalcogenides [14]. Resistive switching can be observed in oxide materials, namely transition metal oxides, when voltage is applied [10]. Organic polymers, due to their varied chemical structures, can display resistive switching behaviour, which shows potential for use in flexible electronics and low-power memory applications [15, 16]. Chalcogenides, which consist of elements from the chalcogen group, exhibit resistive switching and are being investigated for their potential in non-volatile memory due to their unique electrical properties [17, 18]. The collaborative examination of resistive switching in these material categories demonstrates the wide range of variations and

✉ Neeraj Khare
nkhare@physics.iitd.ernet.in

[1] Department of Physics, Indian Institute of Technology Delhi, Hauz Khas, New Delhi 110016, India

[2] Present address: Research & Innovation Center for Graphene & 2D Materials, Khalifa University, Abu Dhabi, United Arab Emirates

potential uses in the developing field of electronic materials and systems [19, 20].

Recently, memory devices utilising nanocomposite samples have emerged as very promising candidate for the next era of memory devices. Nanocomposite samples offer a promising opportunity for utilisation in resistive switching devices, showing enhanced performance characteristics [21]. By incorporating nanoparticles or nanowires into the resistive switching matrix, additional conducting paths are introduced. This enhancement leads to an increase in the switching speed, accompanied by a decrease in power consumption [22]. Moreover, the durability of both the high resistance state (HRS) and low resistance state (LRS) is improved, highlighting the promise of nanocomposite compositions in maximising the efficiency and dependability of resistive switching devices. The properties of nanocomposite samples can be tailored by adjusting the composition size and distribution of nanoparticles or nanowires within the matrix of the material [21, 23–25].

In recent years, the integration of conducting graphitic materials enhances the resistive switching properties, contributing to improved performance and functionality. Conductive graphitic materials such as carbon nanotubes (CNT), graphene oxide (GO), and graphene (Gr) have made significant strides in improving the controllability of the resistive switching characteristics of ReRAM devices. Carbon nanotubes (CNTs) are an excellent material to incorporate into advanced data storage devices because of their exceptional electrical, chemical, and mechanical properties. In addition, carbon nanotubes (CNTs) have a high modulus, remarkable mechanical strength, and large aspect ratio, making them an ideal reinforcing agent for polymers. Deepti et al [26]. reported the effect of CNT in P3HT polymer on the switching property of the device. There was a high ON/OFF ratio ($> 10^2$) and a set voltage of 1.8 V in the memory device containing 4(wt%) CNT in P3HT. Mullani et al. [27]. reported that the TiO_2-CNT composite has resistive switching characteristics, which are dependent on the concentration of the CNT.

Currently, there has been a focus on combining carbon nanotubes (CNT) with oxides due to the coupling of oxides and CNT. This combination offers benefits such as easy processing using solutions and the adaptability to adjust resistive switching based on the material composition [28]. In the present work, the resistive switching behavior zirconium dioxide (ZrO_2) composite structures is studied, which is synthesized through the hydrothermal method. In addition to having a high dielectric constant, a big bandgap, and stable thermal characteristics, ZrO_2 has the potential to be an exciting material for the study of resistive switching [29, 30]. A memory device with a structure consisting of FTO/ ZrO_2-CNT/Ag has been constructed, utilising Ag as the upper electrode and fluorine doped tin oxide (FTO) as the lower electrode. The switching characteristics of the constructed devices with different CNT (wt%) have been investigated. Additionally, the resistance temperature dependency of the memory device at various resistance states was studied. The current voltage (I-V) characteristics of the storage device have been investigated in detail in order to understand the mechanism of resistive switching. Additionally, a potential model has been presented in order to provide an explanation for the observed resistive switching behaviour in the FTO/CNT -ZrO_2/Ag device.The addition of CNT in ZrO_2 is shown to influence the ON/OFF voltage of the nanocomposite resistive switching device.

2 Experimental details

2.1 ZrO_2 synthesis process

Figure 1 shows the schematic of the hydrothermal approach which was utilised for the preparation of the nanostructured ZrO_2 powder. In the beginning, a solution of zirconyl nitrate hydrate $ZrO(NO_3)_2.xH_2O$ having a concentration of 0.5 M was prepared in deionized water. 0.5 M NaOH solution that was prepared in deionized water was gradually added to the zirconyl nitrate solution while the mixture was continuously stirred which was followed by 30 min of sonication to create a uniform solution. 70 ml of the prepared solution was loaded in an autoclave with a capacity of 100 ml fitted with a Teflon lining.

The autoclave was sealed tightly and kept at 180 °C for 24 h before being allowed to cool naturally to room temperature. The precipitate was then filtered, rinsed with distilled water to remove the soluble nitrates and ethanol to decrease agglomeration, and dried at 100 °C for 12 h. This ZrO2 powder was utilised as a precursor in the spray deposition procedure to create a ZrO2 thin film on the FTO substrate.

2.2 Synthesis of carbon nano tubes (CNTs)

Carbon nanotubes (CNT) were synthesized by the thermal chemical vapour deposition method. Briefly, the precursor solution of xylene and ferrocene (0.03 gm/mL) was filled in a quartz boat and kept inside a double-zone furnace at the low-temperature zone. Deposition of the CNT was carried out at 800°C. Afterwards, the as-synthesized MWCNT(Multiwall Carbon Nanotube) were purified by acid treatment to remove the catalyst particles and amorphous carbon, present in the sample. For purification, CNT was firstly dispersed in 6 M HCl and then heated at 80 °C for 24 h. Subsequently, the resulting suspension of the CNT

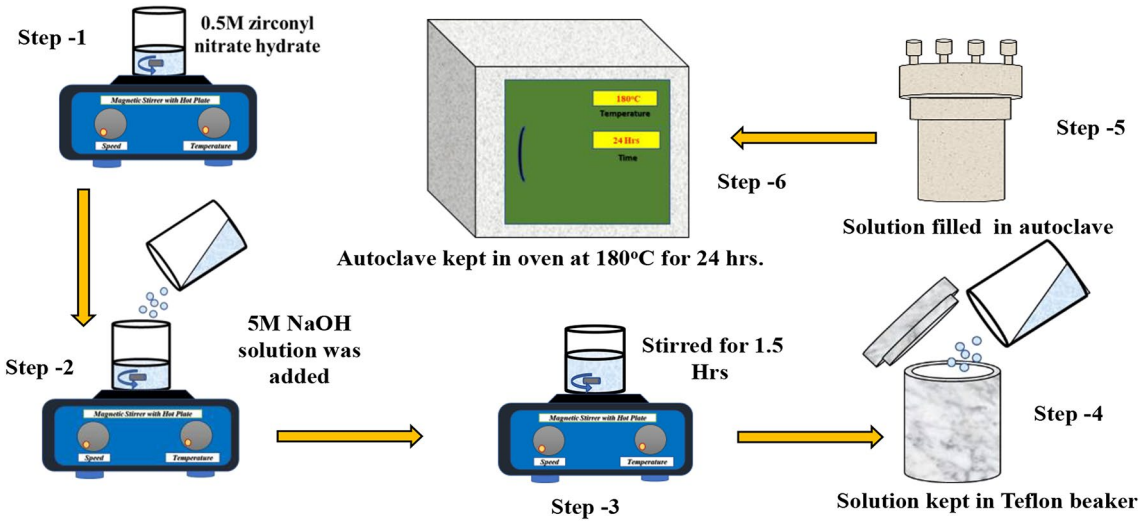

Fig. 1 Schematic of synthesis of ZrO_2 powder

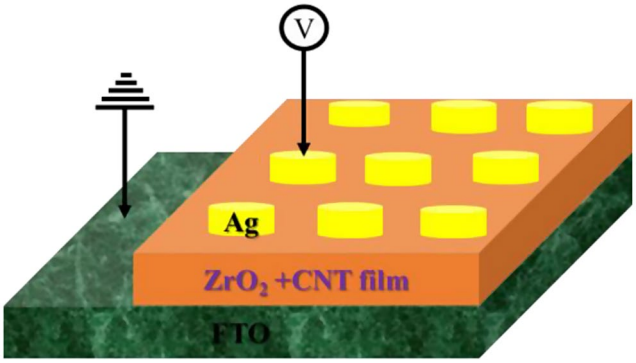

Fig. 2 Schematic of trilayer device FTO/ZrO_2-CNT/Ag

was washed with deionized water and dried at 60 °C for 12 h in an oven.

2.3 Fabrication of device

The tri-layer device as shown in Fig. 2 was fabricated by depositing ZrO_2 or ZrO_2-CNT film using spray coating on the FTO substrate. Initially, the FTO substrate was cleaned using a conventional method [ultrasonication in deionized water acetone and isopropyl alcohol for 10 min each]. After cleaning, a side part of the FTO substrate was covered by kapton tape to have conducting bottom electrode. ZrO_2 powder or ZrO_2-CNT powder was mixed with ethanol and stirred for 30 min. After 30 min of mixing, a diluted citric acid solution was added to the solution. The film of pure ZrO_2 and ZrO_2-CNT was deposited on FTO substrate by spray coating method. Spray coating provides a cost-effective, scalable, and flexible method for depositing ZrO_2 and ZrO_2-CNT films, offering good control over film properties. Integrating carbon nanotubes (CNTs) into ZrO_2 films can improve electrical conductivity, mechanical strength, thermal conductivity, and switching performance [31, 32]. Additionally, it has the potential to reduce the threshold voltage, boost device stability, and improve overall efficiency. The spray-coated ZrO_2-CNT films possess a combination of features that make them extremely well-suited for use in sophisticated resistive switching applications within tri-layer systems.

The resultant solution was kept in a spray gun and was spray coated for 10 min on the FTO substrate. The deposited film was kept at 80°C for an hour. For the preparation of ZrO_2 film, 1wt% CNT and 2wt% CNT were added to ZrO_2 powder. The thickness of the spray-coated film on the FTO substrate was ~250 nm. After the film fabrication, the top Silver (Ag) contact pad of 100 nm thickness was deposited by E-beam evaporation using a shadow mask.

3 Characterizations

3.1 XRD and SEM-EDAX spectra

The properties like electrical conductivity, switching speed, threshold voltage, stability and uniformity of thin film are afftected by nanostructure [33–35]. In order to improve the overall performance of the film, nanostructure crystallite size is optimized by achieving balance between the density of distribution of grain boundaries and defects [36, 37]. A well arranged nanostructure can end up with increased conductivity, lower threshold voltages, and ehanced endurance, rendering the films more appropriate for practical applications. The X-ray diffraction pattern of ZrO_2 and ZrO_2-CNT composite film on FTO substrate is shown in Fig. 3(a) whereas Fig. 3(b) shows SEM pictures and EDAX spectra. The XRD pattern of ZrO_2 film has its characteristic peaks

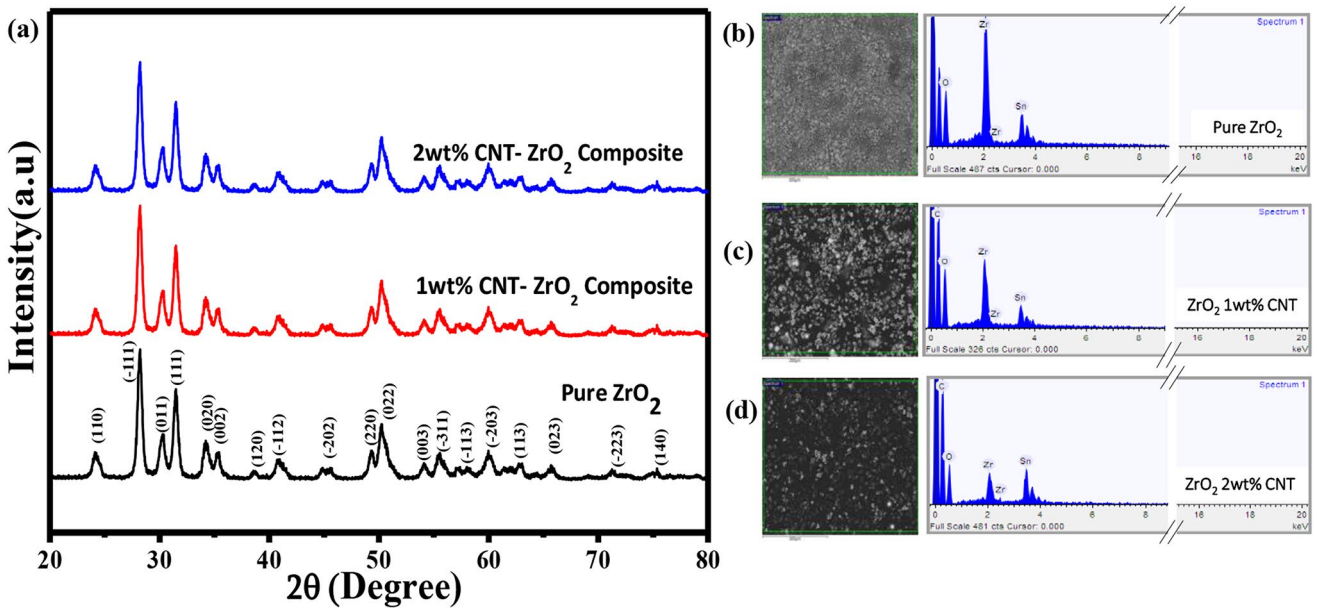

Fig. 3 (**a**) XRD spectra of ZrO_2 and its composite with CNT, (**b**, **c**,**d**). SEM/EDAX spectra of ZrO_2 film, ZrO_2 -1wt% CNT and ZrO_2 -2wt% CNT film respectively

at 24.20°, 28.40°, 30.46°, 31.71°, 34.12°, 35.52°, 38.57°, 40.87°, 44.67°, 49.38° and 50.15° corresponding to (110), (− 111), (011), (111), (020), (002), (120), (− 112), (− 202), (220) and (022) planes, respectively (JCPDS card no. 37–1484). No additional peaks are observed which confirms that single-phase ZrO_2 is present. The XRD diffraction pattern of composite as the small amount of CNT will not affect the ZrO_2 crystal structure. The average crystallite size was equal to ~ 50 nm.

The shape and chemical content of ZrO_2, ZrO_2-1wt% CNT, and ZrO_2-2wt% CNT nanostructures were analysed using SEM and EDAX. Figure 3(b, c,d) shows the surface morphology and EDAX spectra of ZrO_2 and its composites with 1wt% and 2wt% CNT. The surface morphology appear heterogeneous and overlapping due to the aggregation of nanostructures. The EDAX analysis reveals that the ZrO_2 film contains the Zr, and O in appropriate ratio whereas EDAX spectra of ZrO_2-1wt% CNT and ZrO_2-2wt% CNT show the presence of C also along with Zr and O due to presence of CNT.

4 Electrical transport measurement

4.1 I-V and R-T measurements

I-V measurement of all these three devices FTO/ZrO_2/Ag, FTO/1wt% CNT-ZrO_2/Ag, FTO/2wt% CNT-ZrO_2/Ag, and FTO/1wt%CNT-ZrO_2/Ag was performed. Figure 4(a), shows I-V characteristics FTO/ZrO_2/Ag device by scanning the voltage from 0→2→0→-2→0 with step voltage of 0.01 Volts and compliance current (CC) was kept at 1 mA. In the first sweep (0→2) the device stays in HRS till 1.8 Volts and for the applied voltage higher than 1.8 Volts the device switches to LRS in sweep 2 (2→0), the device again stays in LRS during the whole sweep 3(0→-2) whereas for the sweep 4 (-2→0) the device switches from LRS to HRS at -0.8 Volts. Fig 0.5(a) shows, the resistance ratio was HRS and LRS (R_{off}/R_{on}) was ~21.15 at 0.45 Volts. The performance of the device was very stable as it was tested for 100 cycles and the resistance ratio of LRS and HRS remains the same. Figure 4(b) shows the I-V measurement of 1wt% CNT -ZrO_2 composite film with the cycles starting from 0→1→0→-1→0 with compliance current (CC) kept at 10 mA. Initially, in sweep 1(0→1), the device stays in HRS till 0.48 Volts when the voltage is greater than 0.48 Volts the device is turned on and goes to LRS, stays in LRS during the whole sweep 2(1→0) and again it stays in LRS during the whole sweep 3(0→-1), whereas for the sweep 4 (-1→0) the device switches from LRS to HRS at -0.61 Volts.

The resistance ratio of HRS and LRS (R_{off}/R_{on}) was ~37 at a voltage of 0.45 Volts as shown in the Fig. 5.(b). The performance of the device was consistent during the 100 cycles of testing, demonstrating that the resistance ratio of the LRS and HRS remained unchanged. Figure 4(c) shows I-V characteristics of 2wt% CNT-ZrO_2 composite film with sweeping voltage 0 →4→0→-4→0 with applied CC = 100 mA. In sweep 1 (0→4), the device stays in HRS (OFF State) and there is a gradual rise of current at 2.7 Volts when the device goes to LRS, whereas the device stays in LRS during sweep 2 (4→0) and again the device stays in LRS (ON state) during sweep 3(0→-4), a very slight change in current values

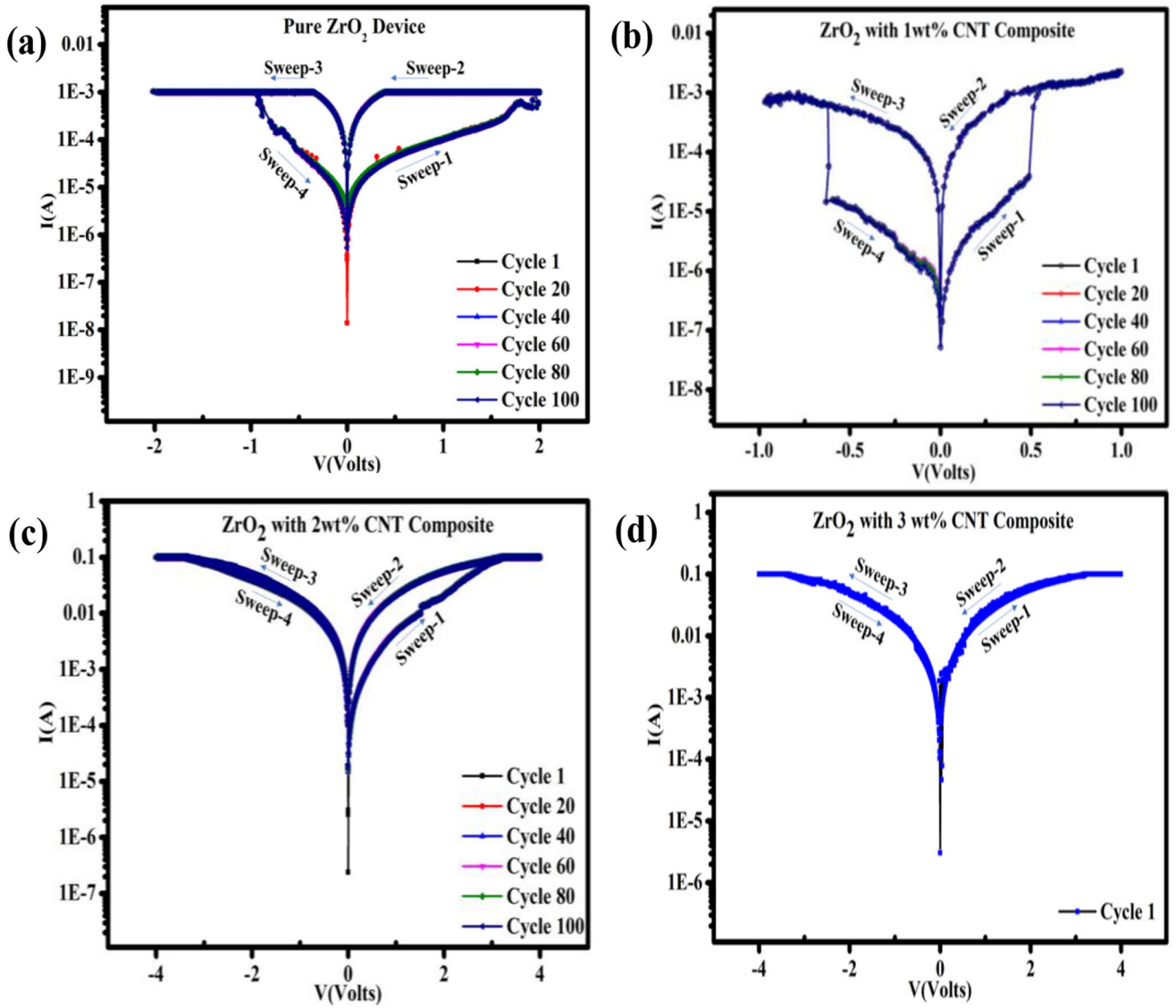

Fig. 4 **(a)** I-V measurement of pure ZrO_2 film, **(b)** 1wt% CNT-ZrO_2 film, **(c)** 2 wt% CNT-ZrO_2 film, **(d)** 3wt% CNT-ZrO_2 film based device

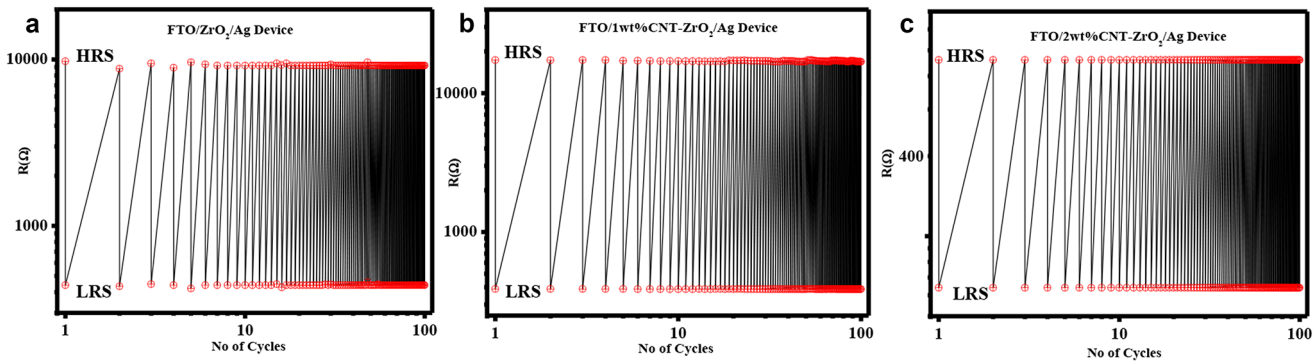

Fig. 5 **(a)** R_{off}/R_{on} ratio of Pure ZrO_2 film, **(b)** 1wt% CNT-ZrO_2 film, **(c)** 2 wt% CNT-ZrO_2 film device

in sweep 4(-4→0) which is very similar to sweep 3(0→-4). Figure 5(c) shows, the resistance ratio of HRS to LRS (R_{off}/R_{on}) was 7 at a voltage of 0.45 Volts. The device stability was confirmed by the fact that its performance did not degrade over the course of 100 cycles, indicating that the resistance ratio between the LRS and HRS did not change. From pure ZrO_2 device I-V measurement, it is clear that the device exhibit forming free rewritable switching behaviour. There is a decrease in the switching voltage for 1wt% CNT-ZrO_2 nanocomposite device and the switching performance is also improved due to the presence of CNT in ZrO_2. For 2wt% CNT-ZrO_2 device no abrupt switching from HRS to LRS was observed, and for 3wt% CNT -ZrO_2 nanocomposite device no switching was observed due to presence of larger amount of CNT conducting filaments might gets formed between the top and bottom electrode.

Similarly Fig. 6 (a, b,c) shows the retention measurement was done for 2 h on pure ZrO_2, -ZrO_2-1wt% CNT, ZrO_2-2wt% CNT film device at 0.45 volts which shows the distinct HRS and LRS values. The distinct HRS and LRS values shows that all the devices are very stable with time and does not show any variation in resistance values with time.

In order to understand the conduction mechanism of the present device temperature dependence of resistance measurement was performed on all the fabricated devices. The LRS and HRS show metallic and semi-conducting behaviour of the fabricated devices respectively. Figure 7(a, b), shows the R-T measurement of a pure ZrO_2 device with an applied voltage of 0.35 volts in HRS (off state) and LRS (on state). The device in HRS shows the semiconducting behaviour with an increase in temperature. The curve was fitted with Arrhenius equation $R = R_0 e^{\frac{-\Delta E}{KT}}$ gives the thermal activation energy as ~50meV. Figure 7(b) shows the R-T curve in LRS(on state). The curves were fitted with the equation $R_T = R_0[1 + \alpha(T\text{-}T_0)]$ where R_T and R_0 are the resistances at the measurement temperature and temperature T_0 respectively, α is the temperature coefficient of resistance. The value of α for the pure ZrO_2 device in LRS estimated from the above equation and was found as 3.1×10^{-3} K^{-1} which indicates that the conduction behaviour is due to the presence of oxygen vacancies [38, 39]. Figure 7(c) shows the R-T measurement for FTO/ ZrO_2-1wt% CNT/Ag device which confirms the semiconducting behaviour present in the device in the HRS with the thermal activation energy as ~42 meV. Figure 7(d) shows the R-T measurement of the FTO/ ZrO_2-1wt% CNT/Ag device. The value of α is estimated as 1.6×10^{-2} K^{-1}. Figure 7(e, f) shows the R-T measurement of FTO/ ZrO_2-1wt% CNT /Ag in both HRS and LRS. In both cases, the device shows metallic behaviour as the resistance increases with the increase in temperature.The value of α for both cases was estimated using an equation, and the values are found as 3.2×10^{-2} K^{-1}, and 4.1×10^{-2} K^{-1} respectively. Figure 8 shows the bar graph for variation of α and E_a values with CNT content in the ZrO_2 matrix. The activation energy is decreased and the value of α is with increased percentage of CNT in ZrO_2 matrix. The higher values of α in the case of LRS of ZrO_2-1wt% CNT, HRS and LRS of ZrO_2-2wt% CNT indicate that the conduction is not only through O_2 vacancies but CNT metallic filaments are also involved.

Figure 9, depicts the schematic of possible mechanisms leading to the low resistance state of ZrO_2 and ZrO_2- CNT nanocomposite device. Figure 9(a) depicts the situation when the ZrO_2 resistive switching device switches to a low resistance state. After the application of voltage, the oxygen vacancies get aligned and form a filamentary connecting path causing the device to switch to LRS.

Figure 9 (b, c,d) shows the effect of CNT in a CNT-ZrO_2 device. Figure 9(b) shows, the effect of CNT causes the growth of CNT filaments and due to this reason the switching voltage is decreased and switching performance is improved in ZrO_2-1wt% CNT device. Figure 9(c, d) shows the increments of CNT conducting filaments as the percentage of CNT is increased. The increase of CNT filaments causes an increase in the conductivity and due to this effect, the switching window is minimized in ZrO_2-2wt% CNT device and finally disappeared in ZrO_2-3wt% CNT device.

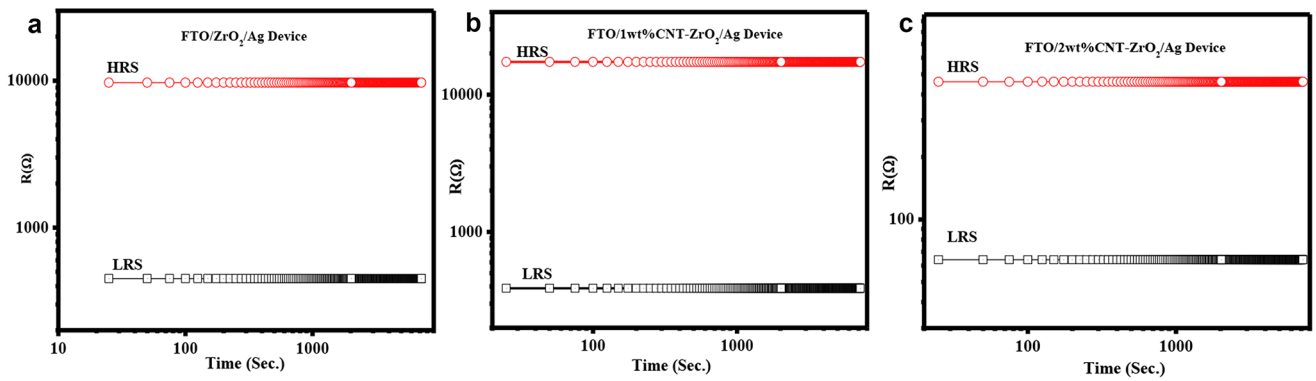

Fig. 6 **(a)** Retentivity measurement of Pure ZrO_2 film, **(b)** 1wt% CNT-ZrO_2 film, **(c)** 2 wt% CNT-ZrO_2 film device

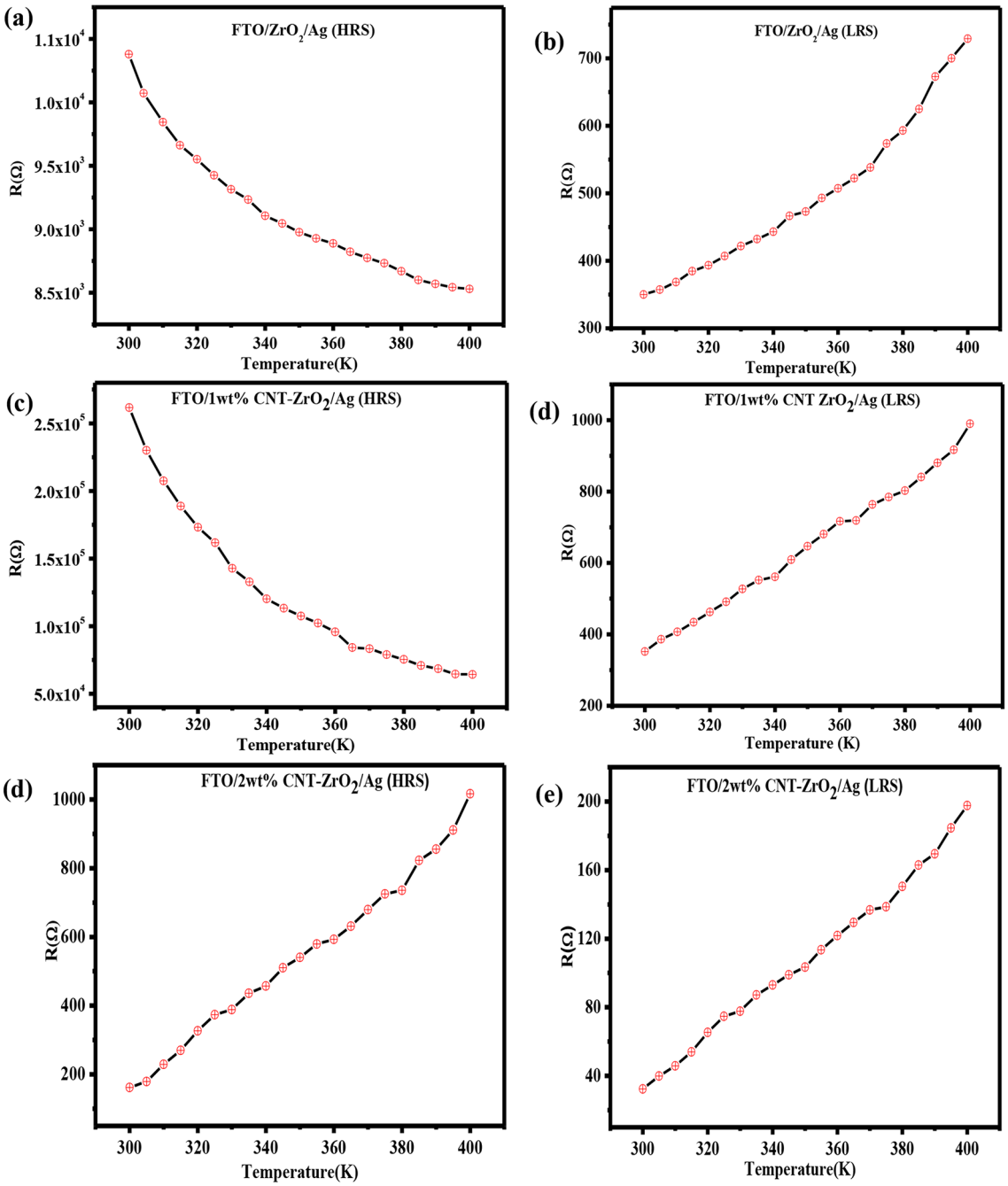

Fig. 7 The temperature dependence of resistance for (**a**) FTO/ZrO2/Ag(HRS), (**b**) FTO/ZrO2/Ag(LRS), (**c**) FTO/1wt%CNT-ZrO2/Ag(HRS), (**d**) FTO/1wt%CNT-ZrO2/Ag(LRS), (**e**) FTO/2wt%CNT-ZrO2/Ag(HRS), (**f**) FTO/2wt%CNT-ZrO2/Ag (LRS)

5 Conclusions

ReRAM devices possess several benefits, such as small power consumption, rapid switching speed, exceptional scalability, and the capacity to retain data without power, which makes them extremely promising for future memory applications. FTO/ZrO_2/Ag and FTO/ZrO_2-CNT/Ag were fabricated using the spray coating method and resistive switching behaviour was studied. Adding 1wt% of CNT to the ZrO_2 film led to switching at lower applied voltages and approximately doubles the resistance ratio between HRS and LRS compared to pure ZrO_2 device. This switching performance is improved due to the presence of CNT in ZrO_2 which causes better conduction between top and bottom electrodes. Nevertheless, surpassing a CNT concentration of 1wt% had a detrimental impact on the switching behaviour. This was attributed to more amount of CNT (2wt%, 3wt%) conducting filaments, resulting in increased conductivity

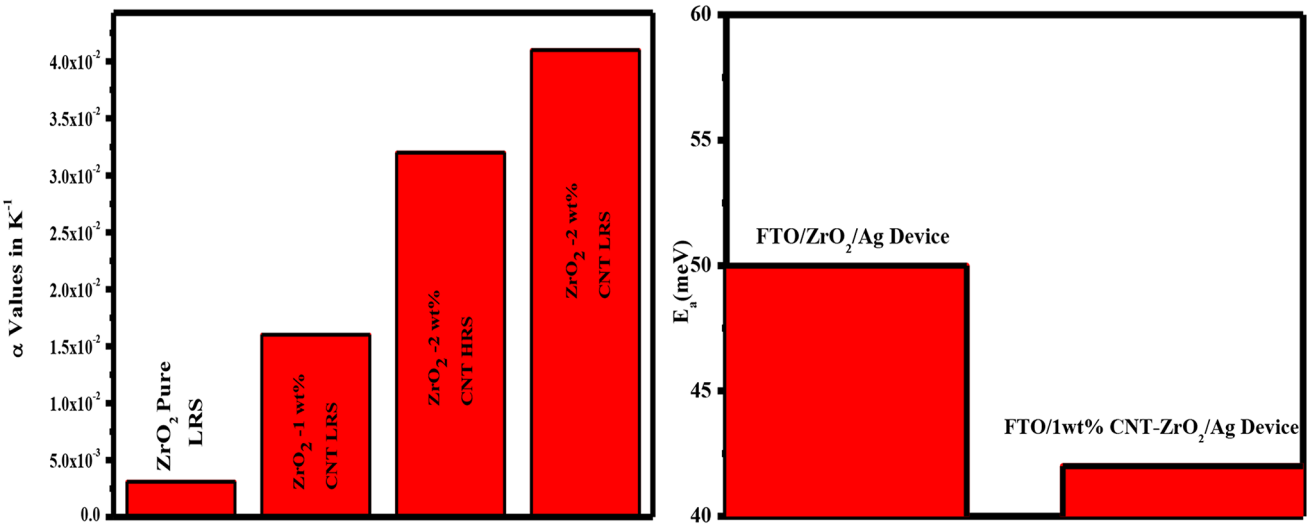

Fig. 8 Variation of α and E_a values with increased percentage of CNT in the host ZrO_2 Matrix

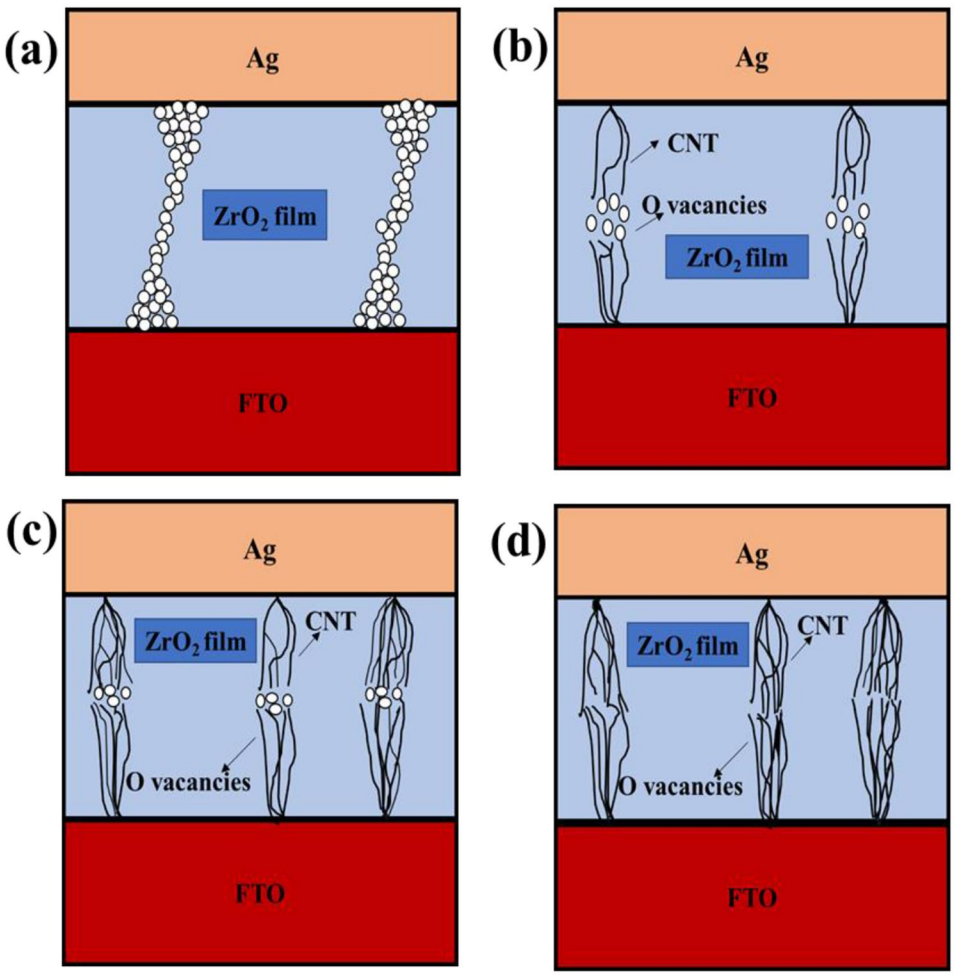

Fig. 9 **a** Conduction mechanism of LRS of (a) pure ZrO_2 device, **(b)** 1wt% CNT- ZrO_2 device, **(c)** 2wt% CNT- ZrO_2 device, **(d)** 3wt% CNT-ZrO_2 device

and a diminished switching window. The comparative R-T analysis revealed that in devices composed only of ZrO_2, only oxygen vacancies were responsible for the formation of conducting filaments. However, in devices including ZrO_2-1wt% CNT, both oxygen vacancies and CNT filaments were found to be aligned between the electrodes. The results emphasize the capability of incorporating carbon nanotubes

(CNTs) into oxide matrices to improve and maximize the resistive switching characteristics of memory devices.

Acknowledgements We would like to express our appreciation to the Ministry of Electronics and Information Technology (project number. RP03530) and the Department of Science and Technology (project no. MI01756) for their contribution of funds to the NNetRA project. Nanoscale Research Facility (NRF) is highly acknowledged for using several characterization facilities.

Author contributions Aman Sharma: Conceptualization (lead), Methodology, Investigation, Writing – original draft, Mohd Faraz: Conceptualization (equal), Writing – original draft, Neeraj Khare: Conceptualization, Supervision, Investigation, Validation, Writing – review & editing.

Data availability No data associated in the manuscript.

Declarations

Competing interests The authors confirm they have no known financial interests or personal connections that could have affected the research presented in this paper.

References

1. A. Moazzeni, H. Riyahi Madvar, S. Hamedi, Z. Kordrostami, Fabrication of Graphene Oxide-based resistive switching memory by the spray pyrolysis technique for Neuromorphic Computing. ACS Appl. Nano Mater. **6**, 2236–2248 (2023)
2. S. Slesazeck, T. Mikolajick, Nanoscale resistive switching memory devices: a review. Nanotechnology. **30**, 352003 (2019)
3. S. Munjal, N. Khare, Advances in resistive switching based memory devices. J. Phys. D **52**, 433002 (2019)
4. S. Munjal, N.J.A.P.L. Khare, Multilevel resistive and magnetization switching in Cu/CoFe2O4/Pt device: coexistence of ionic and metallic conducting filaments, 113 (2018)
5. M. Lanza, F. Hui, C. Wen, A.C.J.A.M. Ferrari, Resistive Switching Crossbar Arrays Based Layer. Mater. **35**, 2205402 (2023)
6. A. Sawa, Resistive switching in transition metal oxides. Mater. Today. **11**, 28–36 (2008)
7. A. Mehonic, S. Cueff, M. Wojdak, S. Hudziak, C. Labbé, R. Rizk, A.J. Kenyon, Electrically tailored resistance switching in silicon oxide. Nanotechnology. **23**, 455201 (2012)
8. G. Dayal, K.J.A.P.A. Jinesh, Correlation between oxygen vacancies and neuromorphic properties of pulsed laser-deposited bismuth iron oxide artificial synapses, **129** (2023) 777
9. E. Shahrabi, T. LaGrange, T. Demirci, Y. Leblebici, Performance improvement of chip-level CMOS-integrated ReRAM cells through material optimization. Microelectron. Eng. **214**, 74–80 (2019)
10. W. Banerjee, A. Kashir, S.J.S. Kamba, Hafnium oxide (HfO2)–a multifunctional oxide: a review on the prospect and challenges of hafnium oxide in resistive switching and ferroelectric memories, **18** (2022) 2107575
11. S.M. Patil, S.S. Kundale, S.S. Sutar, P.J. Patil, A.M. Teli, S.A. Beknalkar, R.K. Kamat, J. Bae, J.C. Shin, T.D.J.S.R. Dongale, Unraveling the importance of fabrication parameters of copper oxide-based resistive switching memory devices by machine learning techniques, **13** (2023) 4905
12. A. Mikhaylov, A. Belov, D. Korolev, I. Antonov, V. Kotomina, A. Kotina, E. Gryaznov, A. Sharapov, M. Koryazhkina, R.J.A.m.t. Kryukov, Multilayer metal-oxide memristive device with stabilized resistive switching, **5** (2020) 1900607
13. K. Krishnan, M. Aono, K. Terabe, T.J.J.o.P.D.A.P. Tsuruoka, significant roles of the polymer matrix in the resistive switching behavior of polymer-based atomic switches, **52** (2019) 445301
14. V. Dhamecha, B. Patel, D. Dhruv, A.J.S.E. Nowicki, Resistive switching memory effects in chalcogenide semiconductor ZnGa2Se4 thin films, **36** (2020) 100–105
15. S. Gao, X. Yi, J. Shang, G. Liu, R.-W.J.C.S.R. Li, Org. Hybrid. Resistive Switching Mater. Devices. **48**, 1531–1565 (2019)
16. J.J.J.o.m.c.C. Ouyang, two-terminal resistive switching memory devices with a polymer film embedded with nanoparticles, **3** (2015) 7243–7261
17. K.O. Čajko, D.L. Sekulić, R. Yatskiv, J. Vaniš, S.J.J.o.N.-C.S. Lukić-Petrović, Impact of Ag concentration in As-S-Se chalcogenide on physical, topological and resistive switching properties, **622** (2023) 122663
18. F. Zhuge, K. Li, B. Fu, H. Zhang, J. Li, H. Chen, L. Liang, J. Gao, H. Cao, Z.J.A.A. Liu, Mechanism for resistive switching in chalcogenide-based electrochemical metallization memory cells, **5** (2015)
19. H.-D. Kim, M.J. Yun, S.J.J.o.t.K.P.S. Kim, Resistive switching characteristics of Al/Si 3 N 4/p-Si MIS-based resistive switching memory devices, **69** (2016) 435–438
20. Y. Gonzalez-Velo, H.J. Barnaby, M.N.J.S.S. Kozicki, Technol. Rev. Radiation Eff. ReRAM Devices Technol. **32**, 083002 (2017)
21. J.H. Lee, C. Wu, S. Sung, H. An, T.W.J.S.r. Kim, Highly flexible and stable resistive switching devices based on WS2 nanosheets: poly (methylmethacrylate) nanocomposites, 9 (2019) 19316
22. Y. Li, S. Long, Q. Liu, H. Lv, M.J.S. Liu, Resistive switching performance improvement via modulating nanoscale conductive filament, involving the application of two-dimensional layered materials, **13** (2017) 1604306
23. J.-Y. Choi, J. Lee, J. Jeon, J. Im, J. Jang, S.-W. Jin, H. Joung, H.-C. Yu, K.-N. Nam, H.-J.J.P.C. Park, High-performance nonvolatile resistive switching memory based on a polyimide/graphene oxide nanocomposite, **11** (2020) 7685–7695
24. A.N. Matsukatova, A.Y. Vdovichenko, T.D. Patsaev, P.A. Forsh, P.K. Kashkarov, V.A. Demin, A.V.J.N.R. Emelyanov, scalable nanocomposite parylene-based memristors: multifilamentary resistive switching and neuromorphic applications, **16** (2023) 3207–3214
25. S. Majumder, K. Kumari, S.J.M.L. Ray, Pulsed voltage induced resistive switching behavior of copper iodide and La0. 7Sr0. 3MnO3 nanocomposites, 302 (2021) 130339
26. D. Chaudhary, S. Munjal, N. Khare, V. Vankar, Bipolar resistive switching and nonvolatile memory effect in poly (3-hexylthiophene)–carbon nanotube composite films. Carbon. **130**, 553–558 (2018)
27. N. Mullani, I. Ali, T.D. Dongale, G.H. Kim, B.J. Choi, M.A. Basit, T.J. Park, Improved resistive switching behavior of multiwalled carbon nanotube/TiO2 nanorods composite film by increased oxygen vacancy reservoir. Mater. Sci. Semiconduct. Process. **108**, 104907 (2020)
28. M. Asif, A.J.M.T.E. Kumar, Resistive switching in emerging materials and their characteristics for neuromorphic computing, **1** (2022) 100004
29. A. Sharma, M. Faraz, P. N.J.T.E.P.J, Khare, Investigation of analog resistive switching in ZrO_2 nanostructured film, **137** (2022) 1–7
30. S.-J. Park, B.-S. Yu, J.-Y. Jeon, B.-C. Kang, T.-J.J.J.o.A. ha, compounds, Sol-gel based zirconium dioxide dielectrics by oxygen-annealing at low temperature for highly stable and robust flexible resistive random access memory, **825** (2020) 154086
31. V.O. Almeida, N.M. Balzaretti, T.M. Costa, M.R.J.N.-S. Gallas, Nano-Objects, enhanced mechanical properties in ZrO2

multi-walled carbon nanotube nanocomposites produced by sol–gel and high-pressure, **4** (2015) 1–8
32. S. Lamnini, D. Pugliese, F.J.C. Baino, Zirconia-Based ceramics Reinforced by Carbon Nanotubes: a review with emphasis on Mechanical Properties, **6** (2023) 1705–1734
33. J.S. Meena, S.M. Sze, U. Chand, T.-Y.J.N.r.l. Tseng, overview of emerging nonvolatile memory technologies, **9** (2014) 1–33
34. Y. Yang, S. Choi, W.J.N.l. Lu. Oxide Heterostructure Resistive Memory. **13**, 2908–2915 (2013)
35. F. Pan, S. Gao, C. Chen, C. Song, F.J.M.S. Zeng, E.R. Reports, Recent progress in resistive random access memories: materials, switching mechanisms, and performance, **83** (2014) 1–59
36. Q. Liu, J. Sun, H. Lv, S. Long, K. Yin, N. Wan, Y. Li, L. Sun, M.J.A.M. Liu, Real-time observation on dynamic growth/dissolution of conductive filaments in oxide-electrolyte-based ReRAM, **24** (2012) 1844
37. S. Munjal, N.J.A.P.L. Khare, Electroforming free controlled bipolar resistive switching in Al/CoFe2O4/FTO device with self-compliance effect, 112 (2018)
38. J. Yu, W. Huang, C. Lu, G. Lin, C. Li, S. Chen, J. Wang, J. Xu, C. Liu, H. Lai, Resistive switching properties of polycrystalline HfOxNy films by plasma-enhanced atomic layer deposition. Jpn. J. Appl. Phys. **56**, 050304 (2017)
39. H.-L. Ma, Z.-Q. Wang, H.-Y. Xu, L. Zhang, X.-N. Zhao, M.-S. Han, J.-G. Ma, Y.-C. Liu, Coexistence of unipolar and bipolar modes in Ag/ZnO/Pt resistive switching memory with oxygen-vacancy and metal-Ag filaments. Chin. Phys. B **25**, 127303 (2016)